Atmospheric Environment 232 (2020) 117511

Contents lists available at ScienceDirect

Atmospheric Environment

journal homepage: http://www.elsevier.com/locate/atmosenv

The impact of volatile organic compounds on ozone formation in the suburban area of Shanghai

Kun Zhang [a,b], Li Li [a,b,*], Ling Huang [a,b], Yangjun Wang [a,b], Juntao Huo [c], Yusen Duan [c], Yuhang Wang [d], Qingyan Fu [c,**]

[a] School of Environmental and Chemical Engineering, Shanghai University, Shanghai, 200444, China
[b] Key Laboratory of Organic Compound Pollution Control Engineering, Shanghai University, Shanghai, 200444, China
[c] Shanghai Environmental Monitoring Center, Shanghai, 200235, China
[d] School of Earth and Atmospheric Sciences, Georgia Institute of Technology, Atlanta, GA, 30332, USA

HIGHLIGHTS

- Characteristics of ambient VOCs and their influences on O_3 formation in a rural area downwind Shanghai were investigated.
- Strong photochemical losses of VOCs, especially alkenes, were found under high O_x concentrations situations.
- Abatement ratio of VOCs/NOx should be no less than 0.72 to effectively control O_3.

ARTICLE INFO

Keywords:
Ozone formation
Volatile organic compounds (VOCs)
Observation-based model (OBM)
Yangtze River Delta

ABSTRACT

Volatile organic compounds (VOCs) are important precursors of photochemical smog and secondary organic aerosol (SOA). Quantitatively assessing the impact of VOCs on ozone (O_3) formation could provide valuable information for the management of emission reduction and photochemical pollution control. In this study, we first figured out the ozone pollution episodes during 2018 at Dianshan Lake (DSL), which is located in the suburban area of Shanghai and is adjacent to three provinces of the YRD region. Then we analyzed continuous variation of O_3 precursors and meteorological parameters. The online measurements show that the average volume mixing ratio of total VOCs (TVOC) was 15.41 ± 11.39 ppbv during the ozone pollution episodes, with the largest contribution from alkanes. To further identify the sources of VOCs, VOC concentration-weighted trajectories (CWT) were analyzed, and the results suggested that Zhejiang province could be the most important source region of VOCs at DSL. Analysis using an observation-base model showed that NO_x and alkenes exhibited the most significant negative and positive influences on O_3 formation, respectively. As for individual species, toluene and isoprene, whose S-weighted concentrations were 6.67×10^{-2} and 5.94×10^{-2} ppbv, respectively, were the key factors promoting the formation of O_3 at DSL. To control the increase of O_3, considering the policy feasibility, the abatement ratio of VOCs/NO_x should be no less than 0.72. The findings advanced our knowledge of VOCs and their impact on O_3 formation and will be helpful in formulating emission control strategies for coping with O_3 pollution in YRD region.

1. Introduction

High levels of ozone (O_3) in urban and regional areas worldwide have long been a major air quality issue (Li et al., 2019; Paoletti et al., 2014; Wang et al., 2009a; Zhang et al., 2019a). In recently years, the O3 pollution has become more and more serious in China. For example, Li et al. (2019) reported severe summertime O_3 pollution and regionally variable trends in about 1000 sites across China from 2013 to 2017. As the major O_3 precursors, volatile organic compounds (VOCs) could contribute to the formation of O_3 through a series of photochemical reactions, including the hydroxyl radical (OH) initiated oxidation of VOCs, nitrogen cycling driven by peroxyl (RO_2) and hydroperoxyl (HO_2) oxidation and photolysis, and the combination of oxygen atom (O) with molecular oxygen (O_2) (Lyu et al., 2016). Therefore, understanding the

* Corresponding author. School of Environmental and Chemical Engineering, Shanghai University, Shanghai, 200444, China.
** Corresponding author.
E-mail addresses: Lily@shu.edu.cn (L. Li), qingyanf@sheemc.cn (Q. Fu).

https://doi.org/10.1016/j.atmosenv.2020.117511
Received 3 January 2020; Received in revised form 8 April 2020; Accepted 13 April 2020
Available online 1 May 2020

characteristics of VOCs is a fundamental process to investigate the influences of VOCs on the formation pathway of O_3. Previous studies suggested that the chemical species and sources of VOCs vary significantly with different areas (He et al., 2019; Lyu et al., 2016; Zheng et al., 2009). For instance, He et al. (2019) suggested that the mean mixing ratio of total VOCs (TVOC) was 34 ± 3 ppbv with largest contribution from alkanes in the Pearl River Delta (PRD) region, while Lyu et al. (2016) found that the TVOC level in Wuhan was relatively low (24.3 ± 0.5 ppbv).

Due to the complicated photochemical reactions in the atmosphere, the relationship between O_3 and its precursors (VOCs and NO_x) is highly nonlinear. A huge number of researches have been carried out to investigate the VOCs-NO_x-O_3 relationship based on observations and/or simulations (He et al., 2019; Lyu et al., 2019; Zhang et al., 2018, 2019a). For a given region, the entire range of VOCs-NO_x-O_3 formation sensitivity could be divided into VOC-limited, NO_x-limited or transition (Wang et al., 2018). Recently, many studies had investigated the mechanism of O_3 formation using observed-based model (OBM) coupled with Master Chemical Mechanism (MCM) (Ling et al., 2017; Lyu et al., 2019; Xue et al., 2014). For instance, Lyu et al. (2019) found the dominant factors influencing O_3 formation could differ sharply at different periods. In addition, the propene-equivalized concentration, maximum incremental reactivity (MIR), O_3 formation potential (OFP) have also been widely used to describe the contribution of VOCs to O_3 formation.

Yangtze River Delta (YRD) region, as a prosperous economic city cluster, has been suffering from severe O_3 pollution in the past few years, as a result of fast economic development and the accompanied intense emissions of O_3 precursors. Given this situation, many studies have been carried out to investigate the formation mechanism of high O_3 levels in the urban areas of YRD region (Gu et al., 2020; Li et al., 2016; Xu et al., 2019). For instance, Li et al. (2016) found O_3 formation at urban Shanghai was VOC-limited by applying ozone source apportionment technology (OSAT) within the Comprehensive Air Quality Model with Extensions (CAMx). In addition, severe O_3 pollution was also observed at the rural areas. However, only limited studies had investigated the cause of high O_3 over rural areas of YRD region (Xing et al., 2017; Zhang et al., 2019a). In those studies, the pattern of O_3 and O_3 precursors were analyzed while relevant photochemical processes were not well studied. Hence, further studies regarding the characteristics of VOCs and the impact of VOCs on O_3 in rural YRD regions are needed.

In this study, the characteristics of ambient VOCs, and their influences on O_3 formation were investigated, based on the data at a rural site in the YRD region from April to September 2018. Combining the concentration-weighted trajectories (CWT) and calculation of initial VOCs concentrations, the potential sources of VOCs emissions were identified. The dominant VOC species affecting photochemical formation of O_3 were quantified using an observation-based box model. The outcomes of this study will be helpful to set up more effective control strategies for dealing with O_3 pollution in the YRD region.

2. Methodology

2.1. Sampling site

The sampling site, namely Dianshan Lake (DSL) air quality monitoring supersite (120.98°E, 31.09°N), is located at the rural area of Shanghai, several hundred meters from Dianshan Lake, with Jiangsu and Zhejiang province lying to the northwest and southwest of it. Fig. 1 shows the location of DSL site. Since the prevailing wind across the YRD region in summer is southeast, this site is usually regarded as the downwind site of Shanghai. Continuous measurements were performed from April 7 to September 25 2018, when the high O_3 episodes occur frequently.

2.2. Measurement of meteorological parameters and criteria air pollutants

The meteorological parameters including temperature (T), relative humidity (RH), atmospheric pressure (P), wind direction (WD) and wind speed (WS) were collected at the DSL supersite (Table 1). All the instruments used for the measurement of gaseous species, i.e., ozone (O_3), nitric oxide (NO), nitrogen dioxide (NO_2), sulfur dioxide (SO_2), carbon monoxide (CO) were housed on top of a 5-floor-high building, about 15 m above ground level. An ultraviolet photometric ozone analyzer (Thermo Scientific, Model 49i), with a method detection limit of 1 ppb

Table 1
Summary of the instruments used in this study.

Parameters	Instrument	Method	Detection limit/ Range/Precision
WS, WD, T, RH	Visala	Meteorological Station	±0.3 m/s, ±3°, ±0.1 °C, ±3%, respectively
O_3	Thermo Scientific, Model 49i	Ultraviolet Photometric	1 ppb (10 s average)
NO, NO2	Thermo Scientific, Model 43i	Chemiluminescence	0.40 ppb (60 s average)
SO2	Thermo Scientific, Model 42i	Pulsed Fluorescence	0.50 ppb (300 s average)
CO	Thermo Scientific, Model 48i	Gas Filter Correlation	0.04 ppm (10 s average)
VOCs	Agilent, GC•866	GC-FID	-

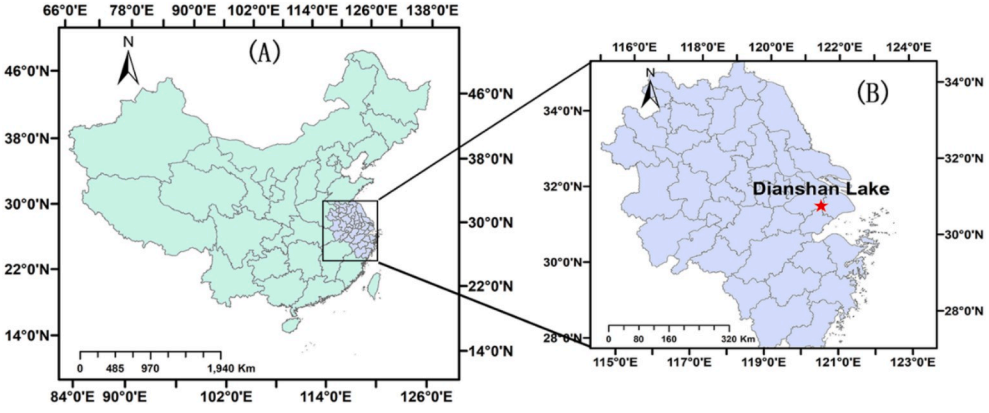

Fig. 1. Location of the Yangtze River Delta region and the DSL supersite (red star). (For interpretation of the references to colour in this figure legend, the reader is referred to the Web version of this article.)

(10 s average) was used to measure the concentration of O_3. NO_x (NO and NO_2) was measured by a NO_x analyzer (Thermo Scientific, Model 43i), with the detection limit of up to 0.40 ppb (60 s average). Concentration of SO_2 was measured by a pulsed fluorescence analyzer (Thermo Scientific, Model 42i), with a detection limit of 0.5 ppb (300 s average). A gas filter correlation analyzer (Thermo Scientific, Model 48i) was used for the measurement of CO. Hourly averaged data of meteorological factors and criteria air pollutants was used in this study.

2.3. Measurement of VOCs

In order to capture the hourly variation of individual VOCs and to obtain abundant data for the subsequent calculation in the observation-based model, a total of 55 VOCs species, including 27 species within C_2~C_6, and 28 species within C_7~C_{12}, were measured by two on-line gas chromatograph (GC) with flame ionization detector (FID) systems. The atmospheric samples were inhaled directly into the system and was preconcentrated by a low carbon (C_2~C_6) analyzer and high carbon (C_6~C_{12}) analyzer, respectively. A built-in auto-calibration system, consisted of three permeation tube (loaded with butane, hexane, and benzene, respectively), was used for daily calibration. The VOC standards gas for photochemical assessment monitoring stations (PAMS) was used to perform monthly calibration for this system. Hourly VOCs data were obtained from this system.

2.4. Estimate of initial concentration of VOCs

VOCs are usually composed of species with high chemical reactivities, especially with OH radicals, and their lifetime range from several hours to several days, depending on their reactivities and the mixing ratio of OH radicals. Hence, the VOCs, which were emitted from various sources, were detected after chemical consumption in the atmosphere. To get a better sense of the original sources of VOCs, the initial mixing ratio of VOCs is required. Several approaches have been developed previously to calculate the initial mixing ratio of VOCs (McKeen et al., 1996; Wiedinmyer et al., 2001). In this study, the approach used in (Kramp and Volz-Thomas, 1997) was adopted, and the description of this approach is given bellow:

$$[AH_i]_t = [AH_i]_0 \times exp(-k_i[OH]\Delta t) \quad (1)$$

where $[AH_i]_t$ and $[AH_i]_0$ is the observed and initial mixing ratio of anthropogenic hydrocarbon i, respectively. k_i is the reaction rate constant of AH_i with OH radicals. [OH] is the mixing ratio of OH radicals. Δt is the reaction time of AH_i. Since the [OH] and Δt are difficult to measure, an estimate of [OH]Δt was used in this study, and the approach is given below:

$$[OH]\Delta t = \frac{1}{k_A - k_B} \times \left(ln\left\{\frac{[A]}{[B]}|_{t=t_0}\right\} - ln\left\{\frac{[A]}{[B]}|_{t=t}\right\}\right) \quad (2)$$

where [A], [B] indicate the mixing ration of VOC_A and VOC_B, respectively. k_A and k_B are the reaction rate constants of VOC_A and VOC_B with OH radicals, respectively. $([A]/[B])_{t=t0}$ is the ratio between initial concentration of VOC_A and VOC_B. Similarly, $([A]/[B])_{t=t}$ is the ratio between observed concentration of VOC_A and VOC_B. To use this method, VOC_A and VOC_B should have similar sources and different reaction rate constant with OH radicals (Wiedinmyer et al., 2001). Since the major loss of VOCs is assumed due to their reaction with OH radicals during daytime (Wang et al., 2013), the average [A]/[B] during nighttime was used for the substitution of $([A]/[B])_{t=t0}$. During the observation, the sunset time was mainly between 17:00 and 19:00, and the photochemical processes after 18:00 could be negligible because of the low solar radical intensity (El-Said and Abdelaziz, 2020; Parra et al., 2019). Hence, we chose a median time, which was 18:00, to roughly represent the average sunset time.

2.5. Concentration weighted trajectory (CWT) model

The concentration weighted trajectory (CWT) model was used in the present study to identify the potential sources of VOCs. This model, based on the pollutant concentration and backward trajectories, had been widely used to identify the potential sources of atmospheric pollutants at a receptor (Bari and Kindzierski, 2018a, b; Liu et al., 2019). The backward trajectories utilized in CWT model were calculated by the National Oceanic and Atmospheric Administration (NOAA) Hybrid Single Particle Lagrangian Integrated Trajectory (HYSPLIT) model (Draxler and Rolph, 2003). The CWT is determined with the following equation:

$$CWT_{ij} = \frac{\sum_{l=1}^{M} C_l \tau_{ijl}}{\sum_{l=1}^{M} \tau_{ijl}} \quad (3)$$

where CWT_{ij} means the average weighted concentration of the trajectory l in the ijth cell, C_l is the observed concentration of a given pollutant in the trajectory l, τ_{ijl} is the resident time of the lth trajectory in the ijth cell (Wang et al., 2009b). To reduce the uncertainty caused by the small values of the number of trajectories loading in ijth cell (n_{ij}), a W_{ij} function was used in this study. The W_{ij} function can be defined as below:

$$W_{ij} = \begin{cases} 1.00 & 80 < n_{ij} \\ 0.70 & 20 < n_{ij} \le 80 \\ 0.42 & 10 < n_{ij} \le 20 \\ 0.05 & n_{ij} \le 10 \end{cases} \quad (4)$$

We use the weighted-CWT_{ij} ($WCWT_{ij} = W_{ij} \times CWT_{ij}$) to describe the potential sources of a given pollutant (Wang et al., 2009b). The global meteorological data used for the calculation of backward trajectories was obtained from NOAA website (http://ftp://arlftp.arlhq.noaa.gov/pub/archives/gdas1).

2.6. Box model

The Framework for zero-Dimensional Atmospheric Modeling (F0AM) coupled with master chemical mechanism (MCM) (Wolfe et al., 2016) was applied to quantify the contribution of individual VOC to local O_3 formation. This model was localized to be applicable in Shanghai, with the setting of latitude, longitude, altitude. The solar zenith angle (SZA) was calculated by this model. This model used the mixing ratio of VOCs, gaseous pollutants and meteorological parameters (such as T, RH, P) as the input for the calculation of photochemical O_3 formation at a given site, based on the master chemical mechanism (version 3.2), which consists of more than 5900 chemical species and 16, 500 reactions. The dilution caused by wind or PBL was parameterized following the function form:

$$\frac{d[x]}{dt} = k_{dil}([x]_b - [x]) \quad (5)$$

where k_{dil} is a first order dilution ration constant and $[x]_b$ is a fixed background concentration. More information about the k_{dil} can be found in the study of Wolfe et al. (2016). The photolysis frequencies (J value) were calculated based on the trigonometric parameterization provided by MCM (Wolfe et al., 2016):

$$J = Icos(SZA)^m \exp(-nsec(SZA)) \quad (6)$$

where I, m, n are constants unique to each photolysis reaction, derived from least-square fits to J values computed with fixed solar spectra and literature cross-section and quantum yields. The selection of cross sections and quantum yields generally follow IUPAC recommendations (Wolfe et al., 2016). As a typical box model, horizonal and vertical transport were not considered.

In this study, the F0AM model was used to assess the sensitivity (S) of

the photochemical production of O_3 to the change of its precursors. The S of a specific precursor X is given by the following equation:

$$S(X) = \frac{[MaxO_3(X) - MaxO_3(X - \Delta X)]/MaxO_3(X)}{\Delta X/X} \quad (7)$$

where X is the concentration of precursor X in the base scenario; ΔX is the hypothetical change of the concentration of X (10% X in this study). $MaxO_3$(X) and $MaxO_3$ (X-ΔX) is maximum value of O_3 in base scenario and the hypothetical scenario. A positive S value of an individual precursor means the O_3 production could be increased if the emission of this precursor increased.

3. Results and discussions

3.1. General statistics

Fig. 2 (A) shows the wind rose during the observation period, suggesting that the wind speed concentrated within 4 m/s and the prevailing wind was southeast. The rainfall flux data during April ~ September was obtained from National Aeronautics and Space Administration (https://www.nasa.gov/) and was exhibited in Fig. 2 (B). Influenced by the summer monsoon, the spatial distribution of rainfall showed an obvious decreasing pattern from south to north (Fig. 2 (B)). During the observation, the rainfall at this site was on average level when compared to other areas in China. Without too much rainfall or drought, this period was suitable for analyzing O_3 formation. Fig. 3 shows the time series of maximum daily 8-h average (MDA8) O_3 concentration, daily average mixing ratio of total VOCs, temperature and relative humidity observed at DSL site from 7 April to 25 September 2018. As is shown in Fig. 3, high O_3 levels (grey shaded period) were always observed when the site was influenced by air masses from southeast. However, strong south wind (yellow shaded period) could also dilute the concentration of air pollutants, leading to relatively lower level of O_3 and other pollutants. During the observation period, the air mass near DSL site was warm and moist (Fig. 3), with the average T and RH of 25.44 ± 5.33 °C and 77.86 ± 17.41%, respectively. High O_3 level (MAD8 > 160 μg/m^3 (or 74.67 ppb, China II standard for O_3) were frequently observed during this period, especially during April 25 ~ April 30, June 11 ~ June 13, July 26 ~ July 30, August 23 ~ August 24, and September 4 ~ September 6. The average MDA8 during this period was 63.67 ± 26.53 ppb, with the maximum value of 131.13 ppb (occurred on 28 April). The average mixing ratio of TVOC was 15.41 ± 11.39 ppbv, with the maximum and minimum value of 112.36 and 2.35 ppbv, respectively. The TVOC level was relatively lower than that observed in the PRD region (He et al., 2019) and Wuhan (Lyu et al., 2016). Consistent with higher O_3 levels, the mixing ratio of TVOCs during O_3 episode days were relatively higher. According to the previous study, if the average measured ratio of VOC (in ppbC) to NO_x (in ppb) during 6:00 am and 9:00 am is more than 8, the local O_3 formation should be in VOC-control regime, otherwise the O_3 formation is in NO_x-control regime (National Research Council, 1991). In this study, the average ratio of VOC/NO_x was 3.96 ± 2.00 (ppbC/ppb). Hence, the local O_3 formation should be in VOC-control regime.

The measured 55 VOCs species included 28 alkanes, 16 aromatics, 10 alkenes and acetylene. During the observation period, the mean mixing ratios of alkanes, alkenes, and aromatics were 9.16 ± 7.39, 2.76 ± 2.98, 3.51 ± 3.46 ppbv, respectively. Table 2 summarizes the top 10 VOC species. Among those VOCs, propane was the most abundant specie (6.67 ± 4.37 ppbv), followed by toluene (1.87 ± 1.26 ppbv), ethylene (1.56 ± 1.03 ppbv), n-butane (1.45 ± 1.06 ppbv), and ethane (1.26 ± 1.14 ppbv). Abundant C3~C5 alkanes, such as propane, n-butane, i-butane and i-pentane, were observed in this site. Propane and n-butane are typical tracers of emissions from liquefied petroleum gas (LPG) or natural gas (NG) combustion, while acetylene and ethylene are key tracers for combustion (Song et al., 2019; Zhu et al., 2018). Therefore, the emission from combustion could be an important source at this site. For the last few years, increasing use of NG was pronounced in YRD, but few control strategies have been applied, which could lead to the emissions from LPG/NG. In addition, toluene and m, p-xylene were listed as the second and eighth abundant VOC species during the observation. The high loading in these aromatics suggested this site could also be influenced by emissions from solvent use or printing processes (Song et al., 2019; Zhang et al., 2019b).

3.2. Photochemical loss of VOCs

As mentioned above, photochemical loss of VOCs can directly affect the observed mixing ratio of individual VOCs. To further evaluate the influence of photochemical processes on VOCs, the photochemical-age-based approach mentioned in section 2.4 was used to estimate the initial concentration of individual VOCs. Different VOC_A and VOC_B were chosen in previous studies. For instance, Parrish et al. (2007) chose n-butane and ethane for the calculation of photochemical age. Wang et al. (2013) and He et al. (2019) used the ratio of ethylbenzene and m, p-xylene ([E]/[X]) to calculate the initial mixing ration of VOCs. In this study, we chose [E]/[X] to calculate the initial concentration of VOCs. The scatter plot of ethylbenzene and m, p-xylene and the result of linear regression in Fig. 4 reveals that there is a strong relationship between ethylbenzene and m, p-xylene, with R value of 0.93 ($p < 0.01$), suggesting the sources of ethylbenzene and m, p-xylene were quite similar. Therefore, [E]/[X] is suitable for the calculation of OH exposure ([OH]Δt). The reaction rate constants of ethylbenzene and m, p-xylene with OH radicals were obtained from the study of (Atkinson and Arey, 2003). Previous studies suggested the value of $([E]/[X])_{t=t0}$ for vehicle

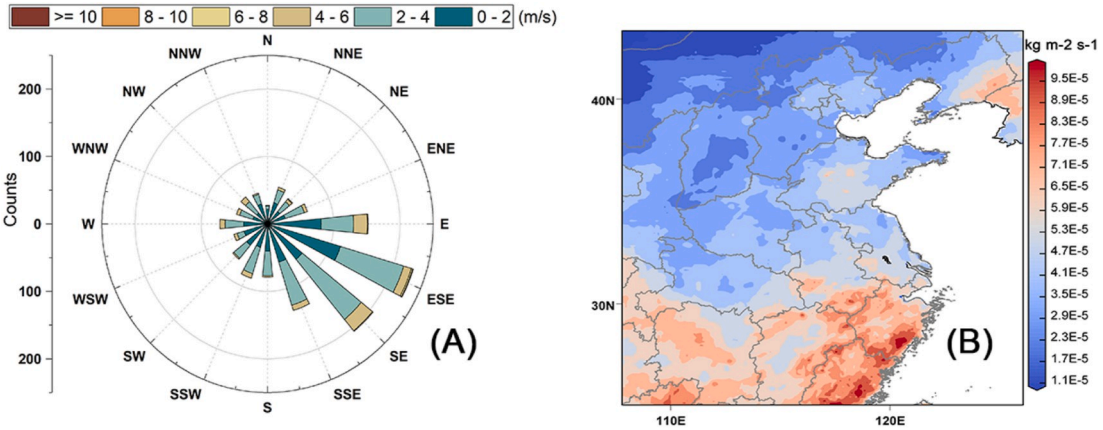

Fig. 2. (A) Wind rose during the observation at DSL site; (B) rainfall flux, in kg m^{-2} s^{-1}, averaged over April ~ September 2018.

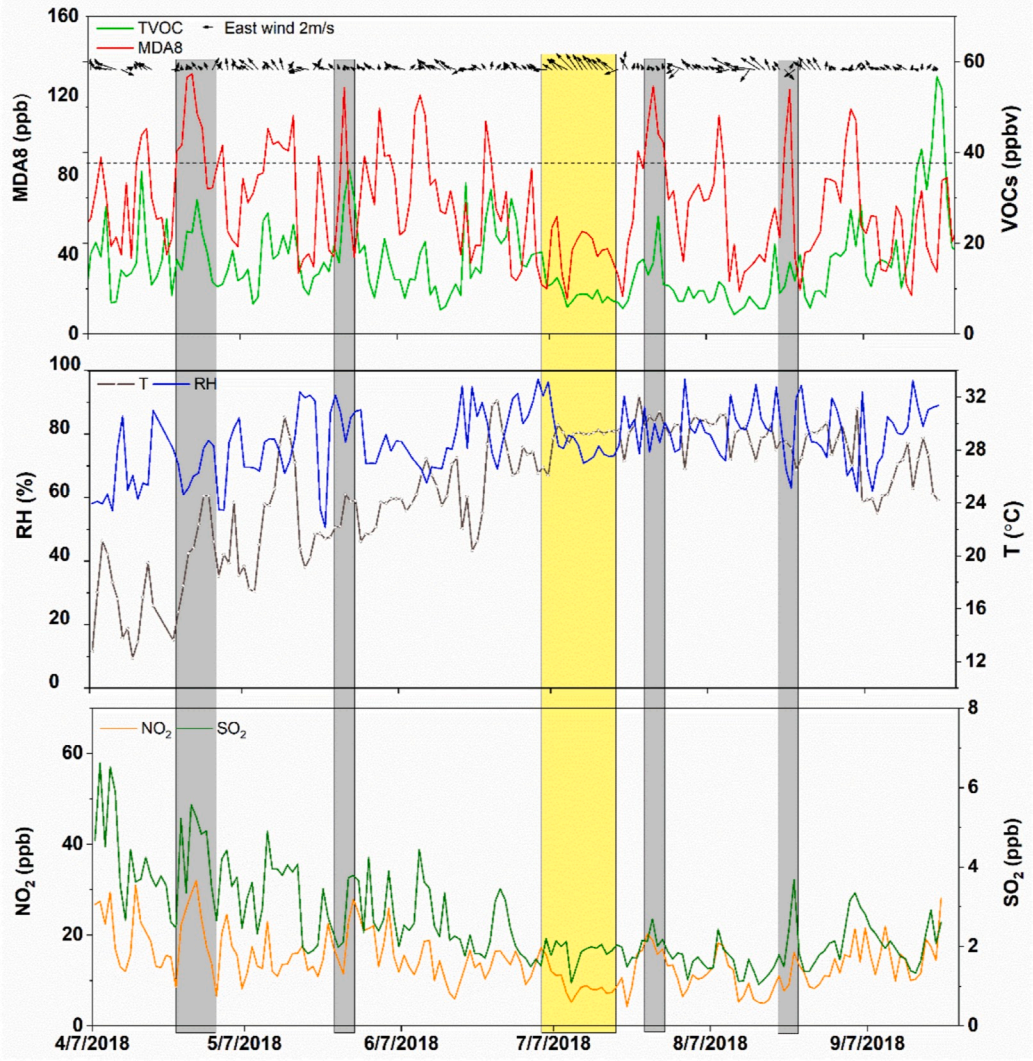

Fig. 3. Time series of VOCs, MDA8, T, and RH observed at DSL site.

Table 2
Summary of top 10 VOCs species during the observation at DSL site.

VOCs	Mean (ppbv)	Median (ppbv)	SD (ppbv)	Max (ppbv)	Min (ppbv)
Propane	2.93	2.33	2.83	38.87	0.25
Toluene	1.87	1.26	1.88	15.64	0.02
Ethylene	1.56	1.03	1.42	10.16	0.00
N-butane	1.45	1.06	1.58	23.40	0.11
Ethane	1.26	1.14	0.86	7.40	0.00
I-butane	0.95	0.72	0.81	7.57	0.09
Acetylene	0.73	0.62	0.50	4.46	0.11
M, p-xylene	0.71	0.54	0.59	3.76	0.04
I-pentane	0.69	0.50	0.61	6.35	0.07
Propene	0.62	0.26	0.99	11.21	0.04

emission and coal combustion to be 0.3–0.4, and about 0.65 for biomass burning (Wang et al., 2013). In the present study, the initial ([E]/[X]) was 0.47, suggesting that the air masses at DSL site were less influenced by biomass burning in the summer season.

The photochemical loss of VOCs was defined as the difference between initial mixing ratio and observed mixing ratio for a given VOCs. Fig. 5 (A) shows the diurnal mean mixing ratio of observed and photochemical loss of alkanes, alkenes, and aromatics from 7 April to 25 September, respectively. During daytime, the highest contribution of

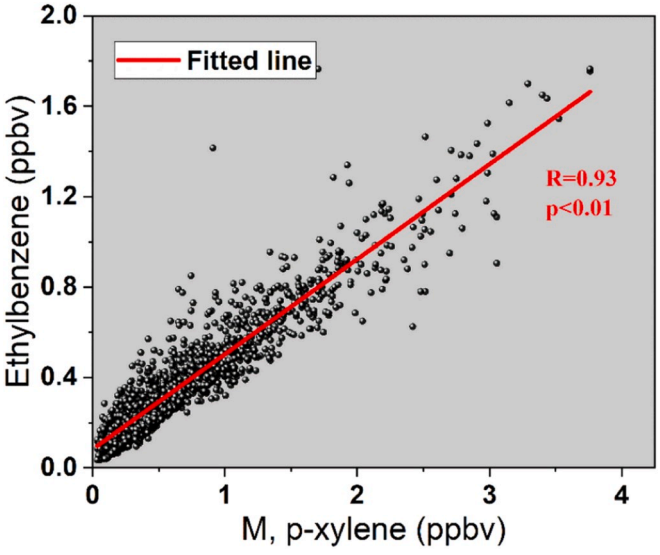

Fig. 4. Scatter plot of ethylbenzene and m, p-xylene at DSL site.

TVOC was from alkanes (8.34 ± 5.36 ppbv, 57.35%), followed by

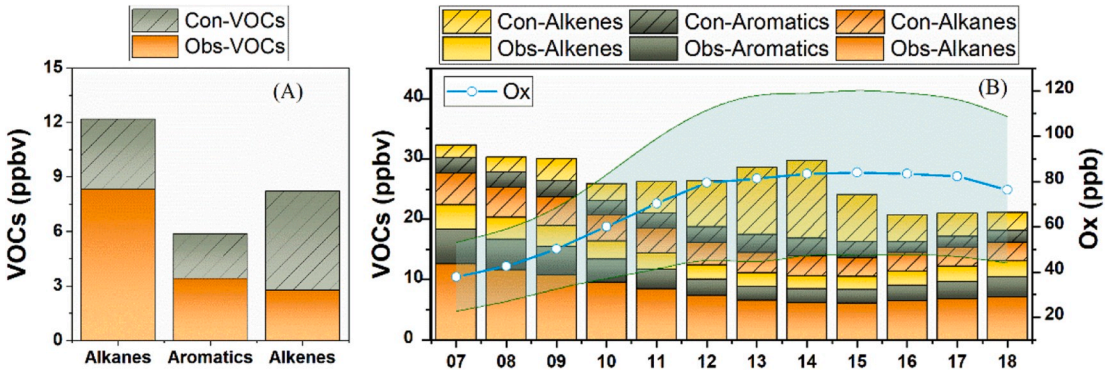

Fig. 5. Daytime variation of observed and consumed VOCs concentrations at DSL site.

aromatics (3.41 ± 2.79 ppbv, 23.53%), and alkenes (2.78 ± 1.77 ppbv, 19.12%). Although the observed mixing ratio of alkenes was the lowest among the three VOC groups, the chemical loss of alkenes was highest (5.44 ± 12.18 ppbv), followed by alkanes (3.86 ± 2.37 ppbv), and aromatic (2.44 ± 2.63 ppbv). The relatively higher consumed values of alkenes were attributed to fast reactions between OH radical and active alkenes.

To obtain the detailed variation of VOCs, we summarized the daytime observed value and photochemical loss value of each VOCs group with a resolution of 1 h (Fig. 5 (B)). Since the atmospheric oxidants (Ox = O_3+NO_2) also exhibit distinct diurnal variations (He et al., 2019), caused by the complicated production and sink process of O_3 and NO_2 in the atmosphere, the diurnal variation of O_x was also given in Fig. 5 to provide insights into the effect of atmospheric oxidizing capacity on the consumption of VOCs. The lowest O_x mixing ratio (37.92 ± 15.20 ppb) occurred at 07:00 a.m., which implied weak atmospheric oxidizing capability, followed by an increasing pattern. Thereafter, O_x reached the maximum value during 14:00 to 15:00, suggesting fast consumption of VOCs. Similar pattern of O_x was also found in the study of (Ismail et al., 2016; Wang et al., 2013; Xu et al., 2011). The maximum observed mixing ratio of VOCs occurred at 07:00 a.m., which could be the joint effects of intensive emissions of VOCs, relatively shallow atmospheric boundary layer (ABL), and the relatively low atmospheric oxidizing ability during morning. Thereafter, a decreasing pattern of observed mixing ratio of VOCs appeared and reached the lowest value at around 14:00, which was usually caused by the development of ABL and the active oxidation processes of VOCs. After 14:00, the observed mixing ratio of VOCs increased gradually as a result of shrink of ABL, decreasing of O_x, and the emission from evening peak. As for the consumption of VOCs, the minimum value (8.02 ± 7.87 ppbv) occurred at 18:00. However relatively higher value of consumed VOCs was found during 12:00 to 15:00, when the O_x was abundant. Among the three VOCs groups, alkenes exhibited the most obvious variation of chemical consumption during daytime, with the maximum and the minimum value of 12.81 ± 23.66 ppbv and 2.05 ± 3.11 ppbv, respectively. As for the consumption of alkenes, trans-2-butene is the highest contributor (3.36 ± 15.41 ppbv, 48.14%), followed by trans-2-pentene, and ethylene.

3.3. Potential sources of ambient VOCs

To identify the sources of air masses influencing DSL during the observation period, the 48-h backward trajectories during daytime were plotted (Fig. 6). The backward trajectories were classified into 3 clusters. Cluster-1 (in red), originating from coastal areas of Zhejiang province and transported slowly to DSL, was the dominant one (62.72%), in which the initial mixing ratios of alkanes, alkenes, and aromatics were 13.65 ± 8.17, 9.93 ± 12.84 and 7.14 ± 5.16 ppbv, respectively. The high loading of VOCs in this cluster suggests the VOCs observed at DSL might mainly originate from Zhejiang province. In addition, the proportion of alkenes in Cluster-1 was the highest (32.32%), indicating the Cluster-1 could be more active than other clusters. More detailed information about the top 10 VOCs species in each cluster is given in Table S2. High levels of reactive alkenes such as trans-2-butene, trans-2-pentene, ethylene, and cis-2-butene were found in Cluster-1. As suggested by Liu et al. (2008), these VOCs were typical tracers of gasoline usage. This is consistent with the huge car ownership in Zhejiang province. The O_3 concentrations in Cluster-1 was the highest, with an average level of 63.07 ± 36.79 ppbv. The abundant reactive O_3 precursors in Cluster-1

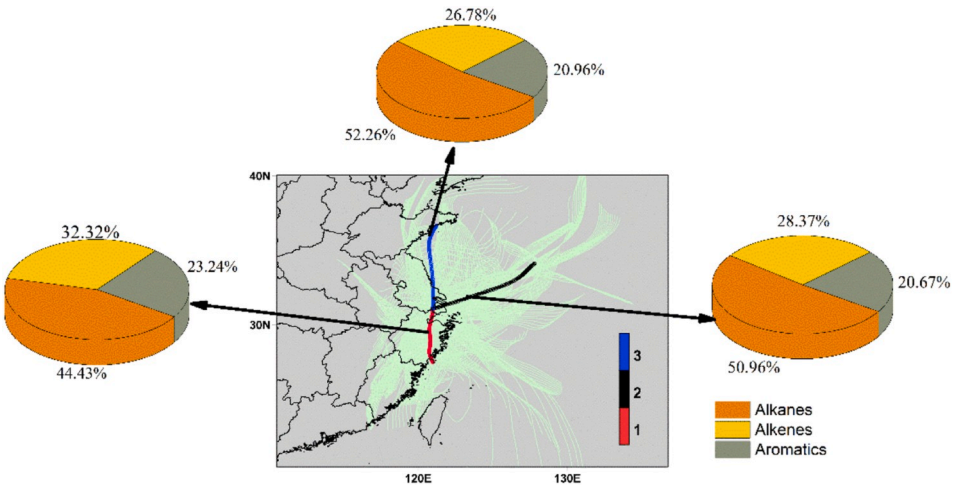

Fig. 6. The 48-h backward trajectories from DSL site and component of initial TVOC in three clusters.

could cause the high O_3 concentration. Custer-2 (in black), accounting for 20.78% of total trajectories, was the cleanest cluster, in which the initial mixing ratios of alkanes, alkenes, and aromatics were only 7.15 ± 2.76, 3.98 ± 7.39, and 2.90 ± 1.19 ppbv, respectively. This suggested that the air mass from East China Sea only contributes a small proportion of TVOC. The mean O_3 concentration in Cluster-2 was only 44.50 ± 19.85 ppbv. Cluster-3 (in Blue), travelling through the Yellow Sea and Jiangsu province, only accounted for 16.50% of the total trajectories. The initial mixing ratios of the three VOC groups were 44.50 ± 19.85 and 56.56 ± 30.09 ppbv, respectively. Relatively high level of i-butane, cis-2-butene, and ethane were found in this cluster. As reported by Liu et al. (2008) and Zhang et al. (2015), use of LPG and vehicle exhaust could be the major sources of these VOCs. The average O_3 concentration in Cluster-3 was 56.26 ± 30.09 ppbv, which was between that in Cluster-1 and Cluster-2. This result suggested that the more the trajectories passing through land, the more active VOCs they may contain, which could further cause higher O_3 concentration in these trajectories.

The potential sources of initial VOCs were identified by the CWT models in this part. A higher WCWT value suggests a region with a higher contribution to the target VOCs group. The WCWT map of initial alkane is shown in Fig. 7. Hot spots of WCWT (>14) were frequently found in Zhejiang, and Jiangsu province, especially near the junction of Zhejiang, Jiangsu, and Anhui province. That could be attributed to summer monsoon, which could transport the alkanes emitted in south China to the monitoring site. In addition, under certain conditions, the alkanes emitted from Jiangsu province could be transported to DSL site by Boreas. As for alkenes, high WCWT value appear along the coastal areas near Zhejiang and Fujian province (Fig. 8). That might be due to the emissions from petrochemical industrial parks located along the coastal areas of Zhejiang province and the Hangzhou bay area. With respect to aromatics, the distribution of WCWT value is similar to that of alkanes. The dominant contribution of initial aromatics is located in Zhejiang province (Fig. 9). Overall, Zhejiang province was the major contributor regarding the sources of initial VOCs at DSL site during the observation period. Hence, to reduce the VOCs concentrations in O_3 episode days at DSL site, regional (especially in Zhejiang province) reduction of VOCs are necessary.

3.4. The impact of VOCs on ozone formation

To assess the roles of different O_3 precursors (VOCs and NO_x) for O_3 formation, we applied F0AM model to the observed VOC concentrations. The observed and simulated O_3 concentrations are shown in Fig. 10, in which the days with insufficient F0AM input data were not shown. Despite the discrepancies, the simulation well caught the pattern of O_3. In this study, we used the index of agreement (IOA) to quantitively evaluate the performance of this model. IOA had been widely used for

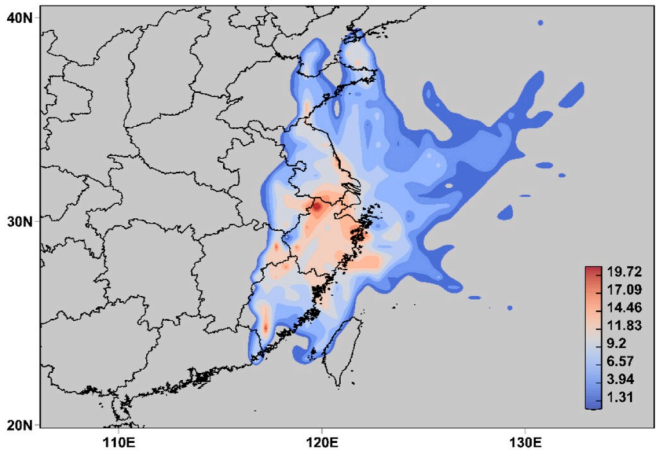

Fig. 7. The WCWT map of initial alkanes.

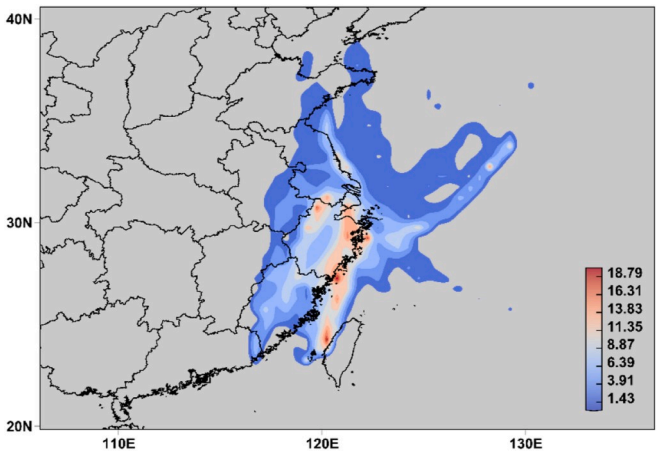

Fig. 8. The WCWT map of initial alkenes.

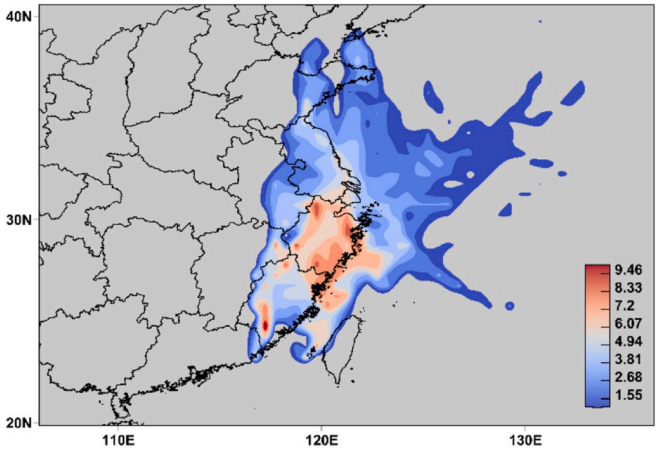

Fig. 9. The WCWT map of initial aromatics.

the evaluation of OBM models and can be calculated by equation (6). Detailed description of IOA can be found in previous studies (He et al., 2019; Lyu et al., 2016, 2019). In the present study, the IOA of O_3 was 0.786, suggesting the model could reasonably reproduce the variation in O_3 and could be used for further analysis. In this model, the dilution of air pollutants was mainly controlled by the k_{dil}, which might be underestimated in certain situations. Therefore, the simulated O_3 concentration would be higher than the observed value.

$$IOA = 1 - \frac{\sum_{n=1}^{n}(O_i - S_i)^2}{\sum_{i=1}^{n}(|O_i - \overline{O}| + |S_i - \overline{O}|)^2} \quad (8)$$

Due to the complexity in atmosphere, O_3 formation could be VOC-limited, NO_x-limited or both-limited in different regions. Therefore, quite different control strategies could be applied in individual area. To preliminarily investigate the potential influence of VOCs and NO_x on O_3 formation, we adopted ozone formation sensitivity (S value). Fig. 11 exhibits the S values of different VOC groups, NO, NO_2 and CO. Clearly the S values of different VOC groups were positive, while that of NO and NO_2 were negative, suggesting that O_3 formation at DSL site was mainly VOC-limited. The implication is that reducing VOCs could lead to O_3 reduction, while cutting NO_x might result in the increase of O_3 at DSL site. Similar VOCs-limited regime was also identified in previous studies (He et al., 2019; Xue et al., 2014; Zeng et al., 2018). Among the three VOC groups, relatively higher S value were found for alkenes, accounting for ~60% of the total S from all VOCs, followed by aromatics (~33%) and alkanes (~7%). The high S value of alkenes indicates that local O_3 formation was more sensitive to changes of alkenes, although

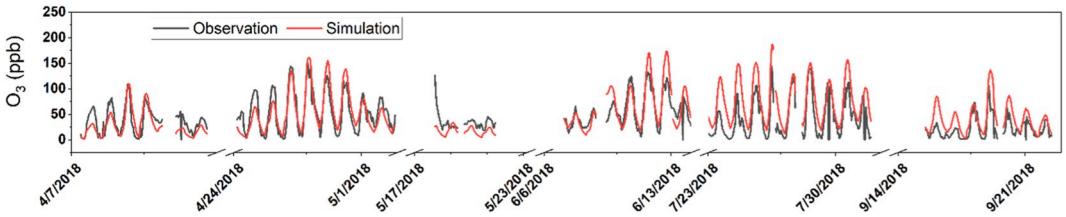

Fig. 10. Comparison of simulated and observed O_3 concentration at DSL site.

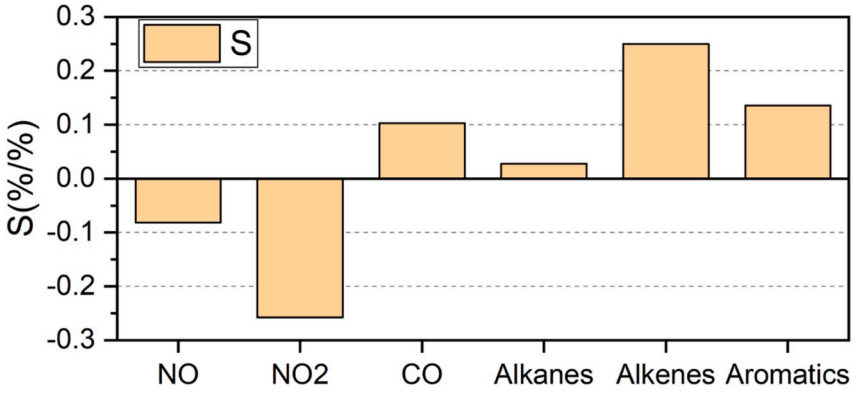

Fig. 11. The S value for different kinds of O_3 precursors.

alkenes only contributed ~19% of observed TVOC. As for NO_2, the large negative S value (−0.26) could be attributed to the reaction between NO_2 and OH radicals (equation (7)), which was considered as an important pathway for O_3 destruction, by which the OH_x radicals and NO_x were effectively consumed, leading indirectly to the reduction of the initial processes of O_3 production (Monks, 2005; Thornton et al., 2002).

$$OH + NO_2 \rightarrow HNO_3 \quad (9)$$

To get an insight into the different influence of detailed VOCs groups on O_3 formation, we calculated the total S values for different VOCs groups according to their carbon number, shown in Fig. 12. As for C_2~C_5 VOCs, the dominant contributor to S value was alkene, suggesting the increase in low carbon olefins could increase the chemical formation of O_3. As indicated by the study of Zhang et al. (2015) and Simayi et al. (2020), low carbon alkenes were tracers of gasoline vehicles. Among C_5 VOCs, isoprene contributed more than 95% of the total S. Since isoprene were mainly from biogenic emission, emission from local vegetation could strongly affect the local O_3 formation. Aromatics contributed the most to the total S value for C_6~C_9 VOCs, since most of the C_6~C_9 species detected in this study were aromatics. Among C_6~C_9 VOCs, toluene, m, p-xylene and 1,3,5-trimethylbenzene were three key species. As suggested by previous studies, these VOCs were usually related to solvent use (Simayi et al., 2020; Yenisoy-Karakaş et al., 2020). High carbon VOCs (such as n-decane, n-undecane, and n-dodecane) were tracers of asphalt application (Liu et al., 2008). Total S values of high carbon VOCs were around 0 since those VOC species were relatively inert. Among all VOCs, the maximum S value (0.19%/%) was observed when carbon number was 5, while the minimum S value occurred when carbon number was 11. This indicated that the O_3 formation from the oxidization process of isoprene was remarkable at this site.

Fig. 13 exhibited the S values for the top 10 abundant VOC species at DSL. Isoprene was found to have the largest S value (0.18%/%) among all VOC species. That was quite different with the results in PRD (He et al., 2019) and Wuhan (Lyu et al., 2016). Isoprene is often used as a tracer of biogenic emissions and given that the vegetation coverage was relatively high around DSL site, O_3 formation is supposed to be sensitive to biogenic emissions. In addition, aromatics, especially m, p-xylene, toluene, ethylbenzene and o-xylene, exhibited relatively higher S value. In order to better quantify the influence of each VOC species on O_3

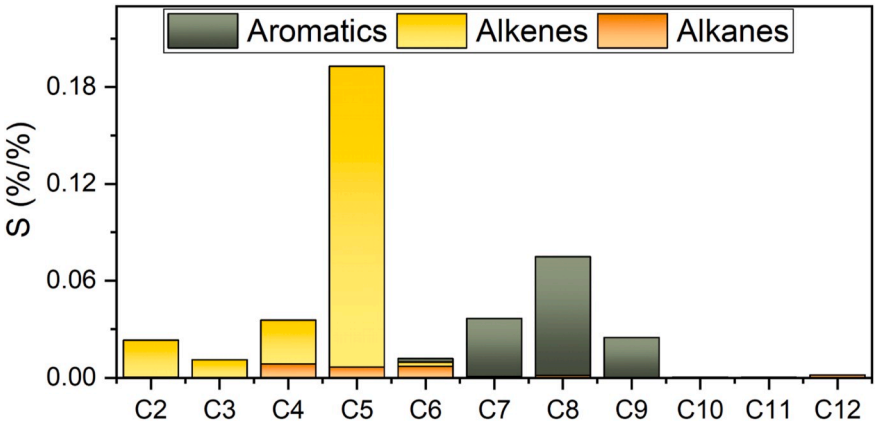

Fig. 12. The S value for different kinds of VOCs (by carbon number).

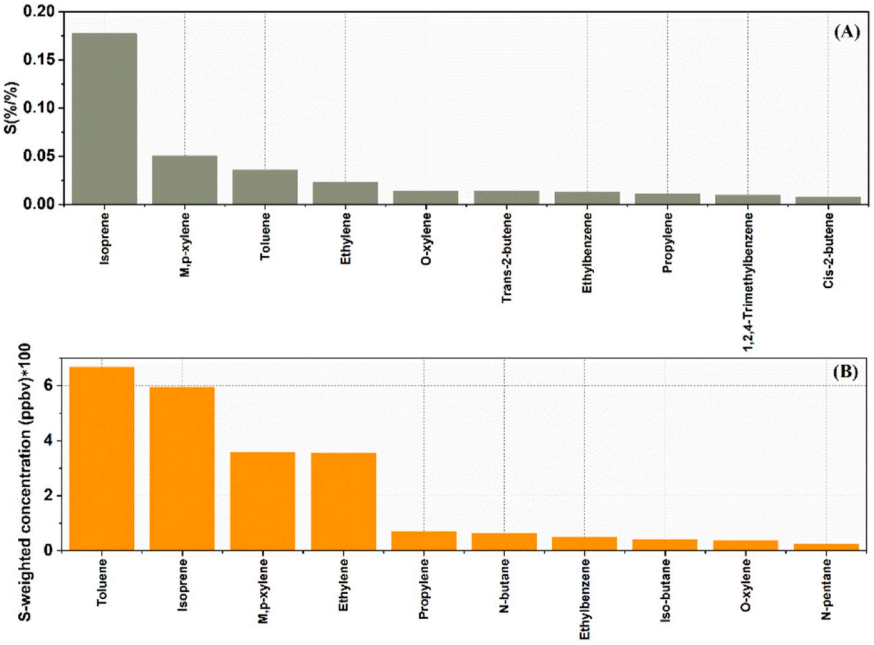

Fig. 13. (A) The S value for individual VOC species, and (B) the S-weighted concentration for individual VOC species.

production, we adopted the S-weighted concentration, which considers both S value and mixing ratio of VOCs (Lyu et al., 2016). The S-weighted concentration of each VOC can be calculated by multiplying its S value with its mixing ratio. The top 10 VOC species in S-weighted concentration is exhibited in Fig. 13 (B). Although toluene only ranked third in terms of S value, it had the most significant influence on the formation of O_3, with a S-weighted concentration of 6.67×10^{-2} ppbv. As for isoprene, even it had the biggest S value, it ranked only second in terms of S-weighted concentration, resulting from the low concentrations in DSL. The S-weighted concentration further revealed that the effect of m, p-xylene and ethylene on ozone formation cannot be neglected, with S-weighted concentration of 3.58×10^{-2} ppbv and 3.55×10^{-2} ppbv, respectively. Since toluene, isoprene, and ethylene were often used as the tracer for solvent-using sources, biogenic sources, and gasoline vehicles sources (Zheng et al., 2009), VOCs-control strategies at DSL site should be targeted for aforementioned sources (excluding biogenic sources).

3.5. Control strategies for ozone episodes

The above analysis demonstrated that O_3 formation was quite sensitive to NO_x and VOCs. However, it was unclear how much VOCs or NO_x should be reduced to achieve effective O_3 improvement, considering the non-linear response of O_3 to changes in VOCs and NO_x emissions. To answer this question, we further conducted series of simulations to calculate the increment of maximum O_3 concentration (Max-O_3) by adjusting input NO_x and VOC ratios. In Fig. 14, the horizontal and vertical axis corresponded to the reduction percentages of NO_x and the increment in Max-O_3 (positive and negative values means the increase and decrease in Max-O_3 compared to the base case), respectively. Each curve in Fig. 14 represents the reduction percentage of VOCs. Results show that the increment of Max-O_3 increased as NO_x reduction increased from 0 to 40%, regardless of the reduction of VOCs. The Max-O_3 decreased gradually when NO_x was cut by >40% in most scenarios, suggesting a transition from VOC-control regime to NO_x-control regime. As for VOCs, a higher cutdown of VOCs always results in more decrease

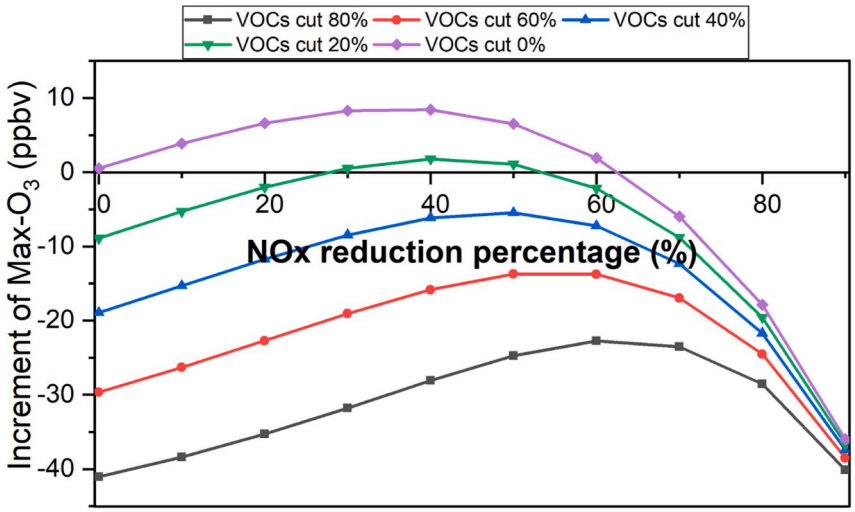

Fig. 14. Reduction of maximum as a function of reduction percentages of NO_x and VOCs.

of Max-O_3 regardless of NO_x. Therefore, when an improper abatement ratio of VOC/NO_x was applied (i.e., when the cut of VOCs is 20%, the increment of Max-O_3 could be negative, positive and again negative when NO_x reduction increased), ozone concentrations could actually go up. Similar pattern was also found in the study of (He et al., 2019). Although great reduction of Max-O_3 could be achieved when VOCs cut was over 60% or NO_x cut was over 70%, it may not be practical in the current stage. Therefore, we focused on the reduction range of 0%–40% for VOCs and 0–70% for NO_x in order to choose optimum control strategies. It was determined that when NO_x reduction was 0–70%, the minimum abatement ratio of VOCs/NO_x for zero Max-O_3 increment (the ratios of VOCs/NO_x at the intersections of the curves and horizontal axis) changed from ~0.38 to ~0.72, suggesting that the minimum abatement ratio of VOCs/NO_x should be higher than 0.72 to prevent the increase in Max-O_3 at the DSL site. That result was relatively lower than that for Wuhan,which was 1.1 (Lyu et al., 2019), suggesting the O_3 formation was less sensitive to the change in NO_x at DSL. In addition, maximum reduction of Max-O_3 (18.94 ppb) could be achieved when the reduction percentages of NO_x and VOCs were 0 and 40%, respectively.

4. Conclusions and policy implications

Based on ground-level observations from April to September 2018 at DSL in YRD, the potential sources of VOCs, ozone formation sensitivities, and the control strategies during O_3 episodes were investigated. The main conclusions are as follows. Strong photochemical losses of VOCs, especially alkenes, were found when O_x concentrations were high. Zhejiang province was found to be the most important potential source region of VOCs at DSL site. Based on the results of scenario analysis, alkenes and NO_2 exhibited the most significant positive and negative influences on O_3 production, respectively. As for individual VOCs, toluene and isoprene were the top two factors promoting O_3 formation.

According to the scenario analysis, reduction of VOCs could lead to a monotonous decrease of Max-O_3. However, improper abatement ratio of NOx and VOCs could lead to the increase of Max-O_3. Therefore, unsuitable control strategies could run counter to what the policymakers want to achieve. Although the results suggest that separate controls on VOCs could bring obvious reductions of Max-O_3, VOCs and NO_x are frequently controlled simultaneously at present. Therefore, the abatement ratio of VOCs/NO_x should be no less than 0.72, considering the policy feasibility, to prevent the increase of O_3 at the DSL site. In addition, the S-weighted concentrations of individual VOCs indicate that the control of solvent-use sources and gasoline vehicles sources could be the most efficient method to reduce O_3 at the DSL site. Overall, this study will be helpful for local and regional policymakers to design appropriate control strategies for O_3 pollution in YRD or other regions of China.

Declaration of competing interest

The authors declare that they have no known competing financial interests or personal relationships that could have appeared to influence the work reported in this paper.

CRediT authorship contribution statement

Kun Zhang: Formal analysis, Writing - original draft. **Li Li:** Writing - review & editing. **Ling Huang:** Formal analysis. **Yangjun Wang:** Formal analysis. **Juntao Huo:** Formal analysis. **Yusen Duan:** Formal analysis. **Yuhang Wang:** Formal analysis. **Qingyan Fu:** Formal analysis.

Acknowledgements

This study was financially supported by the National Natural Science Foundation of China (NO. 41875161), Shanghai International Science and Technology Cooperation Fund (NO.19230742500) and Shanghai Science and Technology Fund (NO.19DZ1205007). We thank Shanghai Environmental Monitoring Center (SEMC) for conducting the measurement and sharing the data.

Appendix A. Supplementary data

Supplementary data to this article can be found online at https://doi.org/10.1016/j.atmosenv.2020.117511.

References

Atkinson, R., Arey, J., 2003. Atmospheric degradation of volatile organic compounds. Chem. Rev. 103, 4605–4638.
Bari, M.A., Kindzierski, W.B., 2018a. Ambient volatile organic compounds (VOCs) in Calgary, Alberta: sources and screening health risk assessment. Sci. Total Environ. 631–632, 627–640.
Bari, M.A., Kindzierski, W.B., 2018b. Ambient volatile organic compounds (VOCs) in communities of the Athabasca oil sands region: sources and screening health risk assessment. Environ. Pollut. 235, 602–614.
Draxler, R.R., Rolph, G.D., 2003. HYSPLIT (HYbrid Single-Particle Lagrangian Integrated Trajectory) Model Access via NOAA ARL READY. NOAA Air Resources Laboratory, Silver Spring. Md website. http://www.arl.noaa.gov/ready/hysplit4.html.
El-Said, E.M.S., Abdelaziz, G.B., 2020. Experimental investigation and economic assessment of a solar still performance using high-frequency ultrasound waves atomizer. J. Clean. Prod. 256.
Gu, Y., Li, K., Xu, J., Liao, H., Zhou, G., 2020. Observed dependence of surface ozone on increasing temperature in Shanghai, China. Atmos. Environ. 221, 117108.
He, Z., Wang, X., Ling, Z., Zhao, J., Guo, H., Shao, M., Wang, Z., 2019. Contributions of different anthropogenic volatile organic compound sources to ozone formation at a receptor site in the Pearl River Delta region and its policy implications. Atmos. Chem. Phys. 19, 8801–8816.
Ismail, M., Abdullah, S., Yuen, F.S., Ghazali, N.A., 2016. A ten-year investigation on ozone and it precursors at Kemaman, terengganu, Malaysia. Environment 9 (1), 1–8.
Kramp, F., Volz-Thomas, A., 1997. On the budget of OH radicals and ozone in an urban plume from the decay of C5-C8 hydrocarbons and NO(x). J. Atmos. Chem. 28, 263–282.
Li, L., An, J., Shi, Y., Zhou, M., Yan, R., Huang, C., Wang, H., Lou, S., Wang, Q., Lu, Q., 2016. Source apportionment of surface ozone in the Yangtze River Delta, China in the summer of 2013. Atmos. Environ. 144, 194–207.
Li, K., Jacob, D.J., Liao, H., Shen, L., Zhang, Q., Bates, K.H., 2019. Anthropogenic drivers of 2013–2017 trends in summer surface ozone in China. Proc. Natl. Acad. Sci. Unit. States Am. 116, 422–427.
Ling, Z., Zhao, J., Fan, S., Wang, X., 2017. Sources of formaldehyde and their contributions to photochemical O_3 formation at an urban site in the Pearl River Delta, southern China. Chemosphere 168, 1293–1301.
Liu, Y., Shao, M., Fu, L., Lu, S., Zeng, L., Tang, D., 2008. Source profiles of volatile organic compounds (VOCs) measured in China: Part I. Atmos. Environ. 42, 6247–6260.
Liu, Y., Song, M., Liu, X., Zhang, Y., Hui, L., Kong, L., Zhang, Y., Zhang, C., Qu, Y., An, J., 2019. Characterization and sources of volatile organic compounds (VOCs) and their related changes during ozone pollution days in 2016 in Beijing, China. Environ. Pollut. 257, 113599.
Lyu, X.P., Chen, N., Guo, H., Zhang, W.H., Wang, N., Wang, Y., Liu, M., 2016. Ambient volatile organic compounds and their effect on ozone production in Wuhan, central China. Sci. Total Environ. 541, 200–209.
Lyu, X., Wang, N., Guo, H., Xue, L., Jiang, F., Zeren, Y., Cheng, H., Cai, Z., Han, L., Zhou, Y., 2019. Causes of a continuous summertime O_3 pollution event in Jinan, a central city in the North China Plain. Atmos. Chem. Phys. 19, 3025–3042.
McKeen, S.A., Liu, S.C., Hsie, E.Y., Lin, X., Bradshaw, J.D., Smyth, S., Gregory, G.L., Blake, D.R., 1996. Hydrocarbon ratios during PEM-WEST A: a model perspective. J. Geophys. Res. Atmos. 101, 2087–2109.
Monks, P.S., 2005. Gas-phase radical chemistry in the troposphere. Chem. Soc. Rev. 34, 376–395.
National Research Council, 1991. Rethinking the Ozone Problem in Urban and Regional Air Pollution. National Academy Press, Washington, D.C, pp. 186–221.
Paoletti, E., De Marco, A., Beddows, D.C., Harrison, R.M., Manning, W.J., 2014. Ozone levels in European and USA cities are increasing more than at rural sites, while peak values are decreasing. Environ. Pollut. 192, 295–299.
Parra, R., Cadena, E., Flores, C., 2019. Maximum UV index records (2010-2014) in Quito (Ecuador) and its trend inferred from remote sensing data (1979-2018). Atmosphere 10 (12), 787.
Parrish, D.D., Stohl, A., Forster, C., Atlas, E.L., Blake, D.R., Goldan, P.D., Kuster, W.C., de Gouw, J.A., 2007. Effects of mixing on evolution of hydrocarbon ratios in the troposphere. J. Geophys. Res. Atmos. 112 (10).
Simayi, M., Shi, Y., Xi, Z., Li, J., Yu, X., Liu, H., Tan, Q., Song, D., Zeng, L., Lu, S., Xie, S., 2020. Understanding the sources and spatiotemporal characteristics of VOCs in the Chengdu Plain, China, through measurement and emission inventory. Sci. Total Environ. 714.
Song, C., Liu, B., Dai, Q., Li, H., Mao, H., 2019. Temperature dependence and source apportionment of volatile organic compounds (VOCs) at an urban site on the north China plain. Atmos. Environ. 207, 167–181.
Thornton, J.A., Wooldridge, P.J., Cohen, R.C., Martinez, M., Harder, H., Brune, W.H., Williams, E.J., Roberts, J.M., Fehsenfeld, F.C., Hall, S.R., Shetter, R.E., Wert, B.P.,

Fried, A., 2002. Ozone production rates as a function of NO_x abundances and HO_x production rates in the Nashville urban plume. J. Geophys. Res. Atmos. 107 (12).
Wang, T., Wei, X., Ding, A., Poon, S.C., Lam, K., Li, Y., Chan, L., Anson, M., 2009a. Increasing surface ozone concentrations in the background atmosphere of Southern China, 1994-2007. Atmos. Chem. Phys. 9 (16), 6217–6227.
Wang, Y., Zhang, X., Draxler, R.R., 2009b. TrajStat: GIS-based software that uses various trajectory statistical analysis methods to identify potential sources from long-term air pollution measurement data. Environ. Model. Software 24, 938–939.
Wang, H., Chen, C., Wang, Q., Huang, C., Su, L., Huang, H., Lou, S., Zhou, M., Li, L., Qiao, L., 2013. Chemical loss of volatile organic compounds and its impact on the source analysis through a two-year continuous measurement. Atmos. Environ. 80, 488–498.
Wang, P., Chen, Y., Hu, J., Zhang, H., Ying, Q., 2018. Attribution of tropospheric ozone to NO x and VOC emissions: considering ozone formation in the transition regime. Environ. Sci. Technol. 53, 1404–1412.
Wiedinmyer, C., Friedfeld, S., Baugh, W., Greenberg, J., Guenther, A., Fraser, M., Allen, D., 2001. Measurement and analysis of atmospheric concentrations of isoprene and its reaction products in central Texas. Atmos. Environ. 35, 1001–1013.
Wolfe, G.M., Marvin, M.R., Roberts, S.J., Travis, K.R., Liao, J., 2016. The Framework for 0-D atmospheric modeling (F0AM) v3.1. Geosci. Model Dev. (GMD) 9, 3309–3319.
Xing, C., Liu, C., Wang, S., Chan, K., Gao, Y., Huang, X., Su, W., Zhang, C., Dong, Y., Fan, G., 2017. Observations of the summertime atmospheric pollutants vertical distributions and the corresponding ozone production in Shanghai, China. Atmos. Chem. Phys. Discuss. 1–31, 2017.
Xu, J., Ma, J.Z., Zhang, X.L., Xu, X.B., Xu, X.F., Lin, W.L., Wang, Y., Meng, W., Ma, Z.Q., 2011. Measurements of ozone and its precursors in Beijing during summertime: impact of urban plumes on ozone pollution in downwind rural areas. Atmos. Chem. Phys. 11, 12241–12252.
Xu, J., Tie, X., Gao, W., Lin, Y., Fu, Q., 2019. Measurement and model analyses of the ozone variation during 2006 to 2015 and its response to emission change in megacity Shanghai, China. Atmos. Chem. Phys. 19, 9017–9035.
Xue, L., Wang, T., Gao, J., Ding, A., Zhou, X., Blake, D., Wang, X., Saunders, S., Fan, S., Zuo, H., 2014. Ground-level ozone in four Chinese cities: precursors, regional transport and heterogeneous processes. Atmos. Chem. Phys. 14, 13175–13188.
Yenisoy-Karakaş, S., Dörter, M., Odabasi, M., 2020. Intraday and interday variations of 69 volatile organic compounds (BVOCs and AVOCs) and their source profiles at a semi-urban site. Sci. Total Environ. 723.
Zeng, P., Lyu, X.P., Guo, H., Cheng, H.R., Jiang, F., Pan, W.Z., Wang, Z.W., Liang, S.W., Hu, Y.Q., 2018. Causes of ozone pollution in summer in Wuhan, Central China. Environ. Pollut. 241, 852–861.
Zhang, Y., Wang, X., Zhang, Z., Lü, S., Huang, Z., Li, L., 2015. Sources of C2-C4 alkenes, the most important ozone nonmethane hydrocarbon precursors in the Pearl River Delta region. Sci. Total Environ. 502, 236–245.
Zhang, K., Xiu, G., Lei, Z., Bian, Q., Duan, Y., Fei, D., Wang, D., Fu, Q., 2018. Vertical distribution of volatile organic compounds within the lower troposphere in late spring of Shanghai. Atmos. Environ. 186, 150–157.
Zhang, K., Zhou, L., Fu, Q., Yan, L., Bian, Q., Wang, D., Xiu, G., 2019a. Vertical distribution of ozone over Shanghai during late spring: a balloon-borne observation. Atmos. Environ. 208, 48–60.
Zhang, X., Yin, Y., Wen, J., Huang, S., Han, D., Chen, X., Cheng, J., 2019b. Characteristics, reactivity and source apportionment of ambient volatile organic compounds (VOCs) in a typical tourist city. Atmos. Environ. 215, 116898.
Zheng, J., Shao, M., Che, W., Zhang, L., Zhong, L., Zhang, Y., Streets, D., 2009. Speciated VOC emission inventory and spatial patterns of ozone formation potential in the Pearl River Delta, China. Environ. Sci. Technol. 43, 8580–8586.
Zhu, H., Wang, H., Jing, S., Wang, Y., Cheng, T., Tao, S., Lou, S., Qiao, L., Li, L., Chen, J., 2018. Characteristics and sources of atmospheric volatile organic compounds (VOCs) along the mid-lower Yangtze River in China. Atmos. Environ. 190, 232–240.